Mon. Not. R. Astron. Soc. **000**, 1–13 (2016) Printed 31 October 2016 (MN LATEX style file v2.2)

Another baryon miracle? Testing solutions to the "missing dwarfs" problem

Sebastian Trujillo-Gomez[1,2⋆], Aurel Schneider[3], Emmanouil Papastergis[4], Darren S. Reed[1,2,5], George Lake[1,2]

[1] *Center for Theoretical Astrophysics and Cosmology, University of Zurich, 8057 Zurich, Switzerland*
[2] *Institute for Computational Science, University of Zurich, 8057 Zurich, Switzerland*
[3] *Institute for Astronomy, Department of Physics, ETH Zurich, Wolfgang-Pauli-Strasse 27, 8093, Zurich, Switzerland*
[4] *Kapteyn Astronomical Institute, University of Groningen, Landleven 12, Groningen NL-9747AD, The Netherlands*
[5] *S3IT, University of Zurich, 8057 Zurich, Switzerland*

arXiv:1610.09335v1 [astro-ph.CO] 28 Oct 2016

Submitted to MNRAS

ABSTRACT

No explanation exists so far for the observed dearth of dwarf galaxies in the local universe compared to the large number of dark matter halos predicted by ΛCDM. Although attempts have been made to attribute the discrepancy to observational systematics, this would require an extreme modification of the density profiles of haloes through baryonic processes. In this paper we perform a systematic evaluation of the uncertainties affecting the measurement of DM halo abundance using galaxy kinematics. Including observational systematics and modelling uncertainties, we derive the abundance of galaxies as a function of maximum circular velocity –a direct probe of mass– from the observed line-of-sight velocity function in the Local Volume. This provides a direct means of comparing the predictions of theoretical models and simulations (including nonstandard cosmologies and novel galaxy formation physics) to the observational constraints. The new "galactic V_{max}" function is steeper than the line-of-sight velocity function but still shallower than the theoretical CDM VF, showing that some unaccounted physical process is necessary to reduce the abundance of galaxies and/or drastically modify their density profiles compared to CDM haloes. Using this new galactic V_{max} function, we investigate the viability of baryonic solutions such as photoevaporation of gas from an ionising background as well as stellar feedback. However, we find that the observed relation between baryonic mass and V_{max} places tight constraints on the maximum suppression from reionisation. Neither energetic feedback nor photoevaporation are effective enough to reconcile the disagreement. This might point to the need to modify cosmological predictions at small scales.

Key words:

1 INTRODUCTION

Dwarf galaxies provide a wealth of information on the formation of the smallest bound structures in the universe. They are also excellent laboratories for understanding the physics that gives rise to galaxies. However, the cosmological properties of dark matter haloes and the observed properties of the galaxies they host can be challenging to disentangle.

A direct way to test the predictions of the cold dark matter model at small scales is to measure the observed abundance of DM haloes. However, since DM is not directly observable, we are left with observable galaxies (and perhaps galaxy voids) as the "peaks of the icebergs" from which to infer the abundance of their host DM haloes. This leads to several complications, including the fact that physical processes such as supernova energy release and photoheating due to reionisation may have a strong effect on the fraction of haloes that host galaxies, as well as on the detectability of these objects.

In the last two decades the cold dark matter model has been confronted with several "small scale" problems. First, the "missing satellites" refers to the underabundance of Milky Way satellite galaxies when compared to the predictions of gravity-only cosmological simulations (Klypin et al. 1999; Moore et al. 1999). Photoevaporation of gas from the lowest mass haloes was presumed to be responsible for the dearth of observed satellite galaxies, although the scale and impact of this process is still under debate (Gnedin

⋆ E-mail: st@physik.uzh.ch

© 2016 RAS

2000; Somerville 2002; Hoeft et al. 2006; Nagashima & Okamoto 2006; Okamoto et al. 2008).

More recently, new measurements of the central mass distributions of these galactic satellites allowed the CDM theory to be tested in more detail. It was found that the central velocity dispersions of the MW dwarf spheroidals are too low to host the most massive dark matter subhaloes predicted by N-body simulations. The so-called "too-big-to-fail" problem is more serious and difficult to solve than the missing satellites because it relates the abundance to the structure of DM haloes using densities instead of luminosities (Boylan-Kolchin et al. 2011). At a given mass or circular velocity, the cosmic abundance of haloes is predicted by cosmology to exquisite precision (e.g., Springel et al. 2005; Diemand et al. 2007; Klypin et al. 2011; Reed et al. 2013; Dutton & Macciò 2014; Hellwing et al. 2016; Heitmann et al. 2016). However, the neglected role of baryons was uncertain and better cosmological tests would require baryonic physics to be included in the models and simulations.

Many solutions to the structure and abundance problems have been proposed since, some involving larger estimates of the mass of the MW, but most invoking a modification of the mass distribution of galactic satellite galaxies through a combination of tidal, ram-pressure stripping, and stellar feedback (e.g., Arraki et al. 2014; Zolotov et al. 2012; Brooks et al. 2013; Brooks & Zolotov 2014; Sawala et al. 2016). Although baryonic effects are now considered to be important in testing predictions of small-scale cosmology, the details and importance of each effect is difficult to assess in a self-consistent manner because of the complexity of the physics involved, and the lack of convergence in the sub-grid models used in hydrodynamics simulations.

Isolated dwarf galaxies are not subject to environmental transformations due to ram pressure and tidal stripping, and hence offer a more direct and clean way of testing cosmological predictions at small scales. ΛCDM predicts the abundance of dark matter haloes to increase steeply with decreasing maximum circular velocity. This galactic velocity function is superior to other abundance probes because it requires no assumptions about the mapping between light and mass.

Surveys have shown that dark matter haloes expected to host galaxies are several times more numerous than observed dwarfs in the local universe. This is the so-called "CDM dwarf overabundance problem" (Tikhonov & Klypin 2009; Zavala et al. 2009; Trujillo-Gomez et al. 2011; Papastergis et al. 2011; Klypin et al. 2015; Papastergis et al. 2015). Klypin et al. (2015) recently used a volume-limited sample of galaxies in the Local Volume to infer the abundance of DM haloes assuming that the observed HI velocity width of galaxies is the same as the maximum circular velocity of their host halo. Other authors have challenged this assumption and find instead that a large correction is necessary (Brook & Shankar 2016; Macciò et al. 2016).

In this paper we develop a novel method to obtain the maximum circular velocity from the observed line-of-sight velocity width using a large, complementary high-quality sample of galaxy rotation curves including the faintest field galaxies studied to date. Using this correction we calculate the abundance of observed galaxies as a function of V_{max}. To make a direct comparison with the observations we include simple models of baryonic effects in the theoretical CDM halo velocity function.

This paper is organised as follows. Section 2 describes the observational data samples and the selection criteria. In Section 3 we describe the method used to correct the observed velocity function from line-widths to halo maximum circular velocities. Section 4 provides functional fits to the abundance of galaxies as a function of V_{max}, and examines the effects of feedback and reionisation on the observed DM halo VF. We discuss our results and present our conclusions in Sections 5 and 6 respectively. Throughout the paper we assume the *Planck* cosmological parameters.

2 DATA AND METHODS

In this paper we use two large and complimentary data sets of gas kinematics, stellar and HI gas mass. The first one is a very deep volume-limited sample of galaxies in the Local Volume. Unfortunately, unresolved HI velocity profiles do not provide the spatial information necessary to fit DM halo density profiles, so we resort to an extension of the resolved kinematics data set from Papastergis et al. (2015) to link the HI profile widths in the volume-limited sample with more detailed kinematic measures. We define baryonic mass as the total stellar plus cold gas mass $M_{\rm bar} = M_{\rm star} + (4/3)M_{\rm HI}$, neglecting molecular hydrogen.

2.1 Local Volume sample

The Local Volume (LV) sample is based on the Karachentsev et al. (2013) catalog. The catalog includes distances, photometry, HI mass estimates, and HI velocity widths for a volume-limited sample of galaxies with distances $D < 10$ Mpc from the Sun. The sample consists of ~ 900 galaxies of all morphological types complete down to a limiting magnitude $M_B = -12$ (Klypin et al. 2015, hereon K15). Assuming $\langle B - K \rangle = 2.35$ (Jarrett et al. 2003) and $M_*/L_K = 0.6$, this corresponds to a stellar mass $\sim 10^{6.8}$ $\mathrm{M}_\odot$.

A subset of 620 objects have both unresolved HI 50 per cent velocity profile width ($W50$) measurements, stellar and HI masses. Most of the late-type galaxies have $W50$ data. For galaxies with HI, the line-of-sight rotation velocity V_{los} is simply $W50/2$, while for those with no detected HI we assume the relation for dispersion dominated galaxies from K15, $V_{los} = 70 \times 10^{-(21.5+M_K)/7}$ km s^{-1} if $M_K < -15.5$, and $V_{los} = 10$ km s^{-1} otherwise. Although this estimate is more uncertain than direct $W50$ velocities, our results are unchanged if we remove these objects from the sample since they constitute less than 10 per cent by fraction.

2.2 Resolved gas kinematics sample

The second data set is an extensive compilation of kinematic HI measurements for 202 gas rich isolated galaxies from a variety of heterogeneous literature sources. Some of these include full rotation curves and some only one published kinematic data point, the outermost measured velocity "$V_{\rm out}$", which corresponds to the deprojected rotation velocity at the maximum measurable radius. All the galaxies in the sample have measurements of HI mass, stellar mass, and 178 have optical half-light radii. For those without half-light radii, we use the fit to the relation between $r_{1/2}$ and $M_{\rm bar}$ from Bradford et al. (2015).

Some of the objects have estimates of the gas velocity dispersion from the original literature sources, while for the rest a constant value $\sigma = 8$ km s^{-1} was added to the deprojected rotation velocity as is customary when modelling the mass distribution (Papastergis et al. 2015),

$$V_{out} \rightarrow \sqrt{V_{out}^2 + 2\sigma^2}. \quad (1)$$

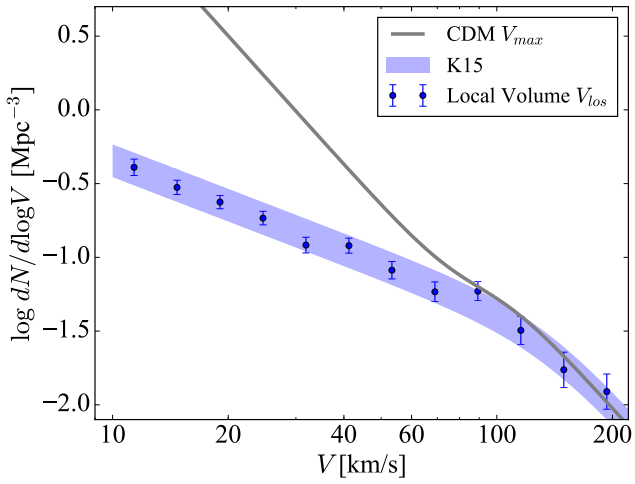

Figure 1. Local Volume line-of-sight velocity function compared to the projected V_{max} velocity function predicted by CDM. The shaded area shows the fit provided by K15 including statistical uncertainty.

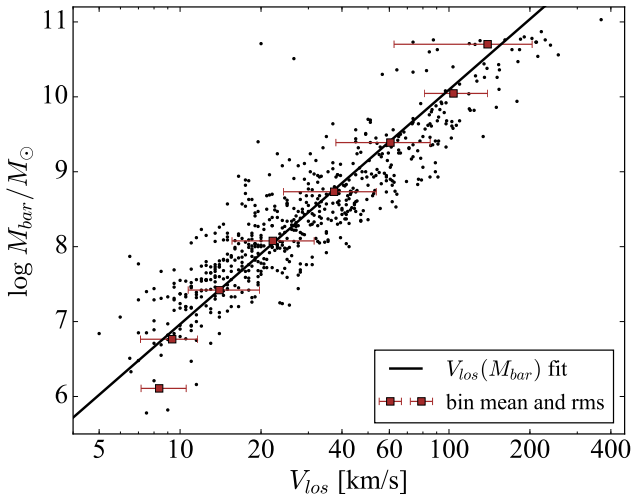

Figure 2. Line-of-sight rotation velocity and baryonic mass for galaxies in the Local Volume sample. Squares with error bars represent the mean and standard deviation of the binned data. The line is a fit of the form $\log V_{los}(M_{\rm bar}) = \alpha \log M_{\rm bar} + \beta$. Despite the large scatter, a linear fit provides a good description of the data, except perhaps for the faintest objects where data is scarce.

In addition to rotation curve data, all the objects also have measured 50 per cent HI profile widths, allowing for direct comparison with the Local Volume data. The sample galaxies span the widest range of velocities and baryonic masses available to date for star forming galaxies, extending down to $M_{\rm bar} \sim 10^6$ M$_\odot$, which is below the completeness limit of the Local Volume sample. For further details we refer the reader to Papastergis et al. (2015) and references therein. From here on we refer to this sample as "P16".

3 ANALYSIS

3.1 The galactic line-of-sight velocity function

The starting point for our analysis is the directly measured galactic line-of-sight velocity function, which is the number density of galaxies as a function of observed HI velocity width (or line-of-sight dispersion in the case of spheroidals). Figure 1 shows the galactic line-of-sight VF in the Local Volume and the V_{max} VF predicted by cold dark matter structure formation. This is essentially the same result that K15 obtained. However, K15 assumed that the correction from V_{los} to the halo V_{max} was negligible, resulting in a large discrepancy between the DM and galactic velocity functions (see Fig. 1).

There are two possible ways to reconcile the observed VF with CDM. Either the rotation velocity of dwarf galaxies severely underestimates the halo maximum circular velocity, or some physical process suppresses the formation of galaxies within DM haloes below 100 km s^{-1}. In this section we consider the first possibility. We need to obtain the maximum circular velocity of each galaxy in the Local Volume by fitting density profiles to kinematic data. However, this requires resolved kinematic data from targeted observations. Most objects in the LV sample do not have rotation curve data so we will need to relate the LV sample line-widths with the resolved rotation velocities of the selected P16 sample.

Our objective here is to find the relation between the galaxy velocity function and the VF of the host DM haloes. Figure 2 shows the total baryonic mass versus V_{los} for the Local Volume sample. The distribution of line-of-sight velocities, correcting for incompleteness as in K15 yields the galaxy velocity function.

To obtain an unbiased description of the relation between $M_{\rm bar}$ and V_{los} we calculate the distribution of the inclination-corrected rotation velocities in bins of $\log M_{\rm bar}$. Figure 2 shows that the resulting binned data can be appropriately described by a linear fit of the form

$$\log V_{los}^{LV} = \alpha \log M_{\rm bar} + \beta, \qquad (2)$$

with $\alpha = 0.32$ and $\beta = -1.22$, and a correlation coefficient $r = 0.897$.

Having shown that the line-width baryonic Tully-Fisher relation of the LV sample is well described by a linear model, we can proceed to relate the line-of-sight HI velocity to the rotation curve measurements necessary for fitting dark matter halo mass profiles.

3.2 Velocity widths and resolved measures of galactic rotation

Similarly to Brook & Shankar (2016), our method relies on directly relating various galaxy kinematic measures via the observed tight coupling with total baryon mass (i.e., the Baryonic Tully-Fisher relation). The scaling between measures of gas rotation and baryon mass has been shown to span a large range of masses from dwarfs to giant discs with very little scatter regardless of whether profile widths or resolved line rotation measures are used (e.g., V_{max} or $V_{\rm flat}$) (McGaugh 2012; Papastergis et al. 2016). Exploiting the relatively small and well-understood systematic errors in the cold baryonic masses of isolated dwarfs (which tend to be gas dominated), we can *statistically* connect the profile widths of Local Volume objects to the outermost resolved rotation measurement, V_{out}, of the P16 sample.

Figure 3 compares the relation between baryonic mass and line-of-sight velocity in the P16 and Local Volume samples. The P16 rotation velocities are well described by a linear model of the form

$$\log V_{rot}^{P16}(M_{\rm bar}) = \delta \log M_{\rm bar} + \gamma, \qquad (3)$$

with $\delta = 0.29$ and $\gamma = -0.80$, and correlation coefficient

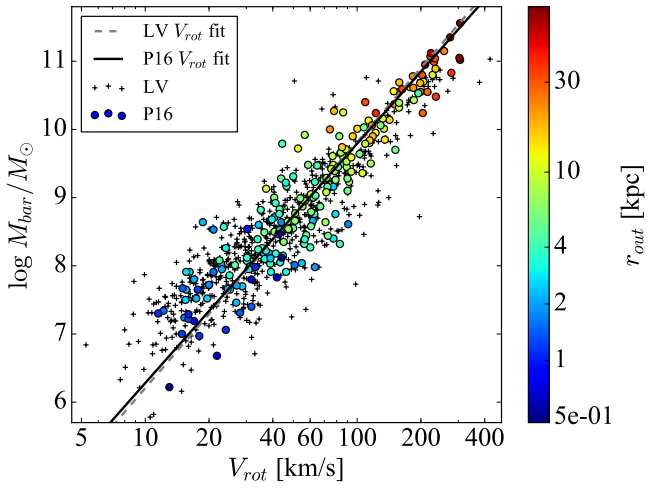

Figure 3. Baryonic Tully-Fisher relation of the P16 selected sample. The rotation velocity is estimated using the HI profile half-width, $V_{rot} = W50/2 \sin i$ to emulate the LV measurements. The colour scale shows the extent of the rotation curve for each galaxy. The plus signs represent the LV sample and its linear fit. The two samples have almost identical BTF relations.

$r = 0.956$. The two data sets are consistent with the same BTFR and scatter. In modelling these data we explicitly assume that for a given baryonic mass the LV and the P16 galaxies inhabit the same dark matter haloes and that systematic deviations in the observed rotation velocities are due to differences in HI content and extent that arise naturally from galaxy formation. Therefore, we can obtain an estimate of the maximum line-width derived V_{rot} of an LV galaxy. Using equations 2 and 3, and assuming that $\langle \log V_{rot}^{LV} \rangle = \langle \log V_{rot}^{P16} \rangle$, gives

$$\langle \log V_{rot}^{LV} \rangle = \langle \log V_{los}^{LV} \rangle + \log \Delta, \tag{4}$$

where

$$\log \Delta = (\delta - \alpha) \log M_{\rm bar} - (\gamma - \beta), \tag{5}$$

and the brackets denote population averages over narrow ranges of baryonic mass.

3.3 Connecting DM halo circular velocities to observed gas kinematics

In the previous section we obtained a statistical correction to calculate the line-width derived rotation velocity V_{rot} at a given line-of-sight velocity V_{los} for Local Volume galaxies. The next step is to find a relation between the V_{rot} of the P16 galaxies and the maximum circular velocity of their host DM haloes.

DM-only N-body simulations in the standard CDM cosmology show that haloes have a density profile well described by the NFW parameterisation (Navarro et al. 1997):

$$\rho(r) = \frac{\rho_0}{\frac{r}{r_s}\left(1 + \frac{r}{r_s}\right)^2}, \tag{6}$$

with

$$r_s = R_{\rm vir}/c, \tag{7}$$

and

$$R_{\rm vir} = \left(\frac{3M_{\rm vir}}{4\pi \Delta_{\rm vir} \rho_{\rm m}}\right)^{1/3}, \tag{8}$$

where $x = r/R_{\rm vir}$, $\Delta_{vir} \approx 335$ is the virial overdensity at present, and $\rho_{\rm m} = 1.36 \times 10^2 \Omega_{\rm m}\ {\rm M}_\odot/\ {\rm kpc}^3$ is the matter density at present. Once the concentration is specified, the NFW profile is uniquely defined for a given $M_{\rm vir}$. To obtain the virial mass we solve the equation for the circular velocity

$$V_{circ}(r) = V_{vir}\left[x \frac{\ln(1+cx) - \frac{cx}{1+cx}}{\ln(1+c) - \frac{c}{1+c}}\right]^{1/2}, \tag{9}$$

and

$$V_{vir} = \left(\frac{GM_{\rm vir}}{R_{\rm vir}}\right)^{1/2}, \tag{10}$$

where $x = r/r_s$. We solve numerically the equation[1]

$$V_{circ}(r_{out}, M_{\rm vir}, c(M_{\rm vir})) = V_{out}, \tag{11}$$

for $M_{\rm vir}$, where $c(M_{\rm vir})$ is obtained from the average concentration-mass relation (Dutton & Macciò 2014)

$$\log c(M_{\rm vir}) = 1.025 \left(\frac{M_{\rm vir}}{10^{12} h^{-1} M_\odot}\right)^{-0.097}, \tag{12}$$

We then obtain the maximum circular velocity[2]

$$V_{max} = V_{circ}(r_{max}), \tag{13}$$

where $r_{max} \approx 2.16 r_s$ for the NFW profile. For an estimate of the uncertainty in the V_{max} we repeat the same calculation for the extreme values of V_{out} and concentration:

$$V_{out}^{\pm} = V_{out} \pm \sigma_{V_{out}} \tag{14}$$

and

$$\log c^{\pm} = \log c(M_{\rm vir}) \mp \sigma_{\log c}, \tag{15}$$

where $\sigma_{\log c} = 1.29$ is the standard deviation in the concentration-mass relation (Dutton & Macciò 2014), and $\sigma_{V_{out}}$ is the reported measurement error in V_{out}. This gives a 1-σ upper limit to the maximum and minimum circular velocity of a halo that could host a galaxy with a given measured V_{out}.

In Appendix B we show that the results presented here do not depend on the relative baryon contribution to the rotation velocity, $(GM_{\rm bar}/r_{out})/V_{out}^2$. Additionally, to guarantee that the DM profiles have not been modified by core formation due to stellar feedback (e.g., Di Cintio et al. 2014; Read et al. 2016), we further limit the sample to galaxies with $r_{out} > 3r_{1/2}$. According to Read et al. (2016) the dark matter distribution should remain unaffected by feedback at $r \gtrsim 2r_{1/2}$. About one hundred galaxies remain in the sample after this selection criteria are applied. The cuts do not significantly affect the main results of the paper (see Appendix A).

Figure 4 shows the Baryonic Tully-Fisher relation of the P16 sample using V_{out} as a probe of rotation velocity. In this case the correlation is also tight, with a scatter $\sigma_{\log V_{out}} = 0.14$ around a linear fit. A fit using only galaxies in the subsample with $r_{out} > 3r_{1/2}$ is essentially identical within the uncertainties to the full

[1] Since massive galaxies are known to have a nonnegligible baryonic contribution to the rotation curve, we subtract the enclosed baryonic mass $V_{out} \rightarrow \sqrt{V_{out}^2 - GM_{\rm bar}/r_{out}}$ when $V_{out} > 100$ km s^{-1}. This assumes that the entire baryonic mass of the galaxy is contained within r_{out}. The approximation is valid since by definition r_{out} occurs near the edge of the HI disc and HI is typically more extended than the stars.

[2] For massive galaxies with $V_{out} > 100$ km s^{-1} we add the baryon mass to the DM fit, $V_{max} = \sqrt{V_{circ}^2(r_{max}) + GM_{\rm bar}/r_{max}}$

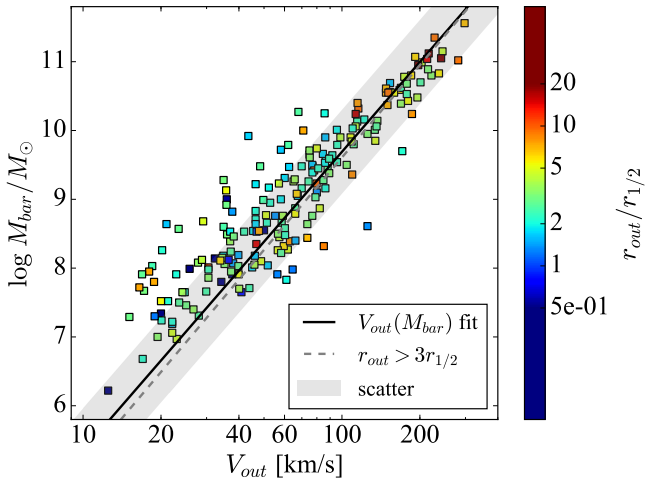

Figure 4. Dependence of the *resolved* P16 BTF relation on the relative extent of the rotation curve. Here the rotation velocity is estimated using the outermost point in the HI rotation curve, V_{out}. The colour scale shows the rotation curve extent relative to the half-light radius for each galaxy. The dashed line shows an error-weighted linear fit including only galaxies with $r_{out} > 3r_{1/2}$, while the solid line shows a fit to the full sample. The sample of galaxies with the most extended kinematic data follows the same BTF relation as the complete P16 sample.

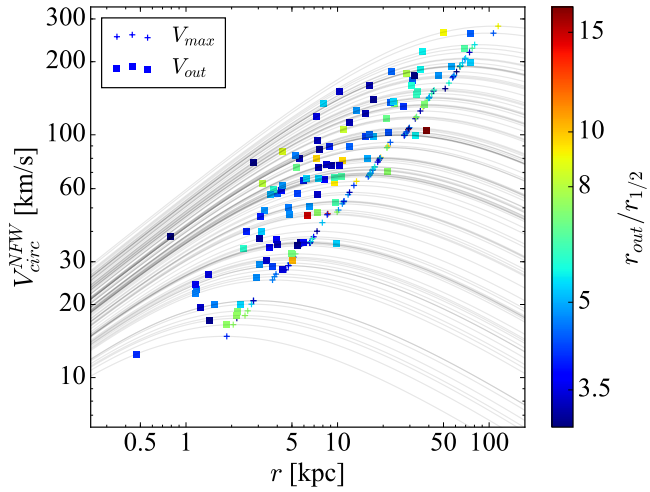

Figure 5. NFW dark matter circular velocity profile fits to the selected P16 subsample. Solid curves show the individual profiles calculated using Eq. 9. The maximum circular velocity of the DM halo is indicated by a plus sign while the outermost point in the rotation curve is represented by a square. Error bars are omitted for clarity.

sample fit. This demonstrates that galaxies with gas discs of relatively different extent all follow the same relation between baryonic mass and rotation velocity. In other words, there is no systematic bias in the selection of the subsample used for profile fitting.

The DM halo profiles obtained for the P16 subsample are shown in Figure 5. In several galaxies the fitted circular velocity profile reaches V_{max} at or near the outermost point in the rotation curve. However, for many, the profile keeps rising and the maximum can be at several times r_{out}. Figure 5 shows that the difference between V_{out} and V_{max} is in general small but not negligible. Thus, the assumption by K15 that the difference between V_{rot} and V_{max} is less than 30 percent applies generally and agrees with our conclusions.

The last step in the procedure is to find a statistical correction to obtain the galaxy V_{max} from the observed HI rotation velocity. In Figure 6 we plot the relation between these two quantities in the selected P16 subsample.

The figure also shows the total uncertainties from measurement error as well as halo concentration as error bars. To avoid biases, we calculate the statistics of the error-weighted data in uniform $\log V_{rot}$ bins and perform a fit to the mean V_{max} of the binned data. The data is well described by a linear model of the form

$$\langle \log V_{max} \rangle = \zeta \langle \log V_{rot}^{\rm P16} \rangle + \eta, \qquad (16)$$

with $\zeta = 0.89$ and $\eta = 0.22$ and rms scatter $\sigma_{V_{max}} = 0.09$. As expected, massive galaxies with $V_{rot} > 80$ km s^{-1} are well fit by haloes with V_{max} close to the measured inclination-corrected HI profile half-width. For smaller galaxies, the HI gas does not seem to extend far enough to probe the maximum circular velocity of the halo, resulting in a larger correction as V_{rot} decreases. The mean correction is less than 5 km s^{-1} for dwarf galaxies with $V_{rot} \approx 12$ km s^{-1}.

Using Eq. 16 together with Eqs. 2 and 3 we can now derive a relation between the line-of-sight rotation velocity of a galaxy in

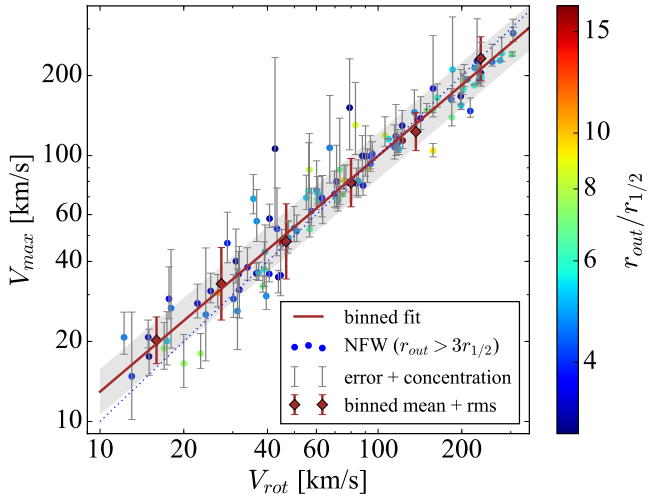

Figure 6. Galaxy maximum circular velocity V_{max} as a function of observed inclination-corrected rotation velocity in the P16 selected subsample. Circles with thin error bars represent individual galaxies and their total uncertainties (due to measurement and concentration, Eqs. 14 and 15). The colour scale shows the maximum extent of the rotation curve relative to the half-light radius. Diamonds with thick error bars denote the mean and standard deviation of the error-weighted V_{max} values in uniform $\log V_{rot}$ bins. The solid line is a linear fit to the binned data. The shaded area shows the scatter in V_{max}. The dotted line indicates the relation $V_{max} = V_{rot}$.

the Local Volume and its maximum circular velocity,

$$\langle \log V_{max}^{\rm LV} \rangle = \langle \log V_{los}^{\rm LV} \rangle + \log \Delta, \qquad (17)$$

where

$$\log \Delta = (\zeta\delta - \alpha) \log M_{\rm bar} + (\zeta\gamma + \eta - \beta), \qquad (18)$$

and angled brackets denote population means over narrow $M_{\rm bar}$ bins.

4 RESULTS

4.1 The abundance of galaxies as a function of V_{max}

Equation 17 allows us to assign a V_{max} to each object in the LV based on detailed modelling of the density profiles of the P16 sample galaxies. Although we apply this correction to each object individually, the resulting V_{max} is only meaningful in a statistical interpretation when an ensemble average is calculated.

Another issue that arises is the intrinsic scatter in the BTF relations. It is possible to repeat our analysis by modelling the scatter analytically in Eq. 17. However, our method is simpler and does not require assumptions about the error distributions which can affect the slope of the VF (i.e., through Eddington bias).

Figure 7 shows our main result, the V_{max} velocity function in the Local Volume. The distribution is well fit by a Schechter function of the form

$$\Phi(V_{max}) = \frac{dN}{d\log V_{max}} = \phi^* \left(\frac{V_{max}}{V^*}\right)^p \exp\left[-\left(\frac{V_{max}}{V^*}\right)^q\right], \quad (19)$$

with $\phi^* = 2.72 \times 10^{-2}$ Mpc^{-3}, $V^* = 2.50 \times 10^2$ km s^{-1}, $p = -1.13$, and $q = 3.14$. This fit is also shown in Figure 7. The V_{max} Function is slightly steeper than the observed V_{los} VF but still shallower than the CDM VF because the difference between the halo V_{max} and the measured rotation velocity is small and increases as galaxy mass decreases. The galactic V_{max} function we obtain here should be used as a benchmark for any structure formation model to reproduce in order to be considered successful at small scales. In the next section we evaluate the effects of baryonic processes on the theoretical CDM velocity function to determine its ability to predict the abundance of small structures.

4.1.1 *The effect of feedback-induced cores on the observed V_{max} function*

Galaxy formation simulations with very efficient supernova feedback implementations typically produce dwarf galaxies with DM density profiles that are shallower than NFW in the inner few kiloparsecs (e.g., Mashchenko et al. 2008; Governato et al. 2010, 2012; Teyssier et al. 2013; Di Cintio et al. 2014; Trujillo-Gomez et al. 2015; Oñorbe et al. 2015; Read et al. 2016; Tollet et al. 2016). However, the details of the transformation are still a matter of debate. For example, Di Cintio et al. (2014) parameterise the core-creation efficiency solely as a function of the ratio $M_{\rm star}/M_{\rm halo}$, while Oñorbe et al. (2015) and Read et al. (2016) find that it also depends on the star formation history of the galaxy. The extent and slope of the DM core is also debated.

Recently, Read et al. (2016) found that the effect of supernova feedback is converged once the resolution is high enough to properly capture the expansion of the blastwave. They provide a general modification of the NFW profile,

$$M_{\rm coreNFW}(<r) = M_{\rm NFW}(<r) \times \left[\tanh\left(\frac{r}{r_c}\right)\right]^n, \quad (20)$$

where

$$n = \tanh\left(\kappa \frac{t_{\rm SF}}{t_{\rm dyn}}\right), \quad (21)$$

and $t_{\rm SF}$ and $t_{\rm dyn}$ are the total star formation time and the circular orbit time at the NFW scale radius respectively. Their simulations are well fit with $\kappa = 0.04$. Furthermore, Read et al. (2016) show that this "coredNFW" profile fits problematic rotation curves within CDM. For an effectively flat core, the parameter

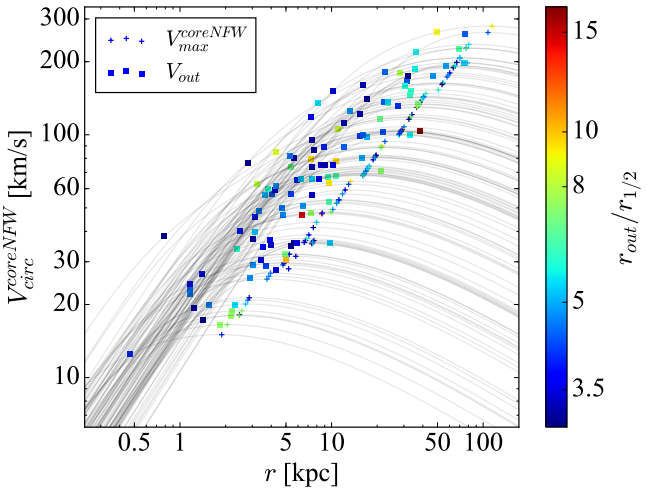

Figure 8. Same as Fig. 6 but for cored NFW profiles obtained using the prescription from Read et al. (2016).

$t_{\rm SF} >> t_{\rm dyn}$ and $n = 1$. The core radius is proportional to the projected stellar half-mass radius, $r_c = 1.75R_{1/2}$. The circular velocity of the coredNFW profile becomes

$$V_{circ}^{\rm coreNFW}(r) = V_{circ}^{\rm NFW}(r) \times \left[\tanh\left(\frac{r}{r_c}\right)\right]^{n/2}. \quad (22)$$

We repeat the same profile-fitting procedure from Section 3.3 replacing Equation 11 with

$$V_{circ}^{\rm coreNFW}(r_{out}, M_{\rm vir}, c(M_{\rm vir})) = V_{out}, \quad (23)$$

and solving for $M_{\rm vir}$ while assuming $R_{1/2}$ is equal to the half-light radius for each galaxy. In Appendix C we show that the particular choice of cored profile parameterisation has no effect on our results.

Figure 8 shows the resulting cored DM halo fits. Although the central circular velocities are reduced with respect to Figure 5 due to the presence of a core, the maximum circular velocity of the haloes stays relatively unchanged. This is a result of our selection of the P16 subsample with $r_{out} > 3r_{1/2}$. We emphasize here that these fits represent an extreme case where all galaxies form the most extreme shallow DM cores seen in simulations irrespective of their stellar mass. These V_{max} values thus represent upper limits to the effect of feedback on the V_{max} velocity function in our analysis.

Figure 9 shows the $V_{max} - V_{rot}$ relation of the selected P16 galaxies assuming extreme feedback-induced cores.

The result is essentially unchanged from Figure 7 because of the cut we imposed on the extent of the rotation curve data. Ensuring that $r_{out} > 3r_{1/2}$ selects galaxies for which a DM core does not modify the rotation curve at the outermost point. Is is important to note that performing the profile fits to galaxies with smaller $r_{out}/r_{1/2}$ would place some galaxies in very massive haloes. This is because at a fixed circular velocity in the inner region, a cored profile will have larger $M_{\rm vir}$ (see, e.g., Papastergis et al. 2016). We assume these solutions are unphysical since they probably correspond to haloes that are not cored due to their small $M_{\rm star}/M_{\rm halo}$.

We have shown that observational effects and dark matter halo cores cannot account for the large discrepancy in the abundance of Local Volume galaxies compared to CDM haloes. However, theoretical work has shown that other important effects should be included when computing the theoretical abundance of galaxies hosted by DM halos. In the following section we evaluate the ef-

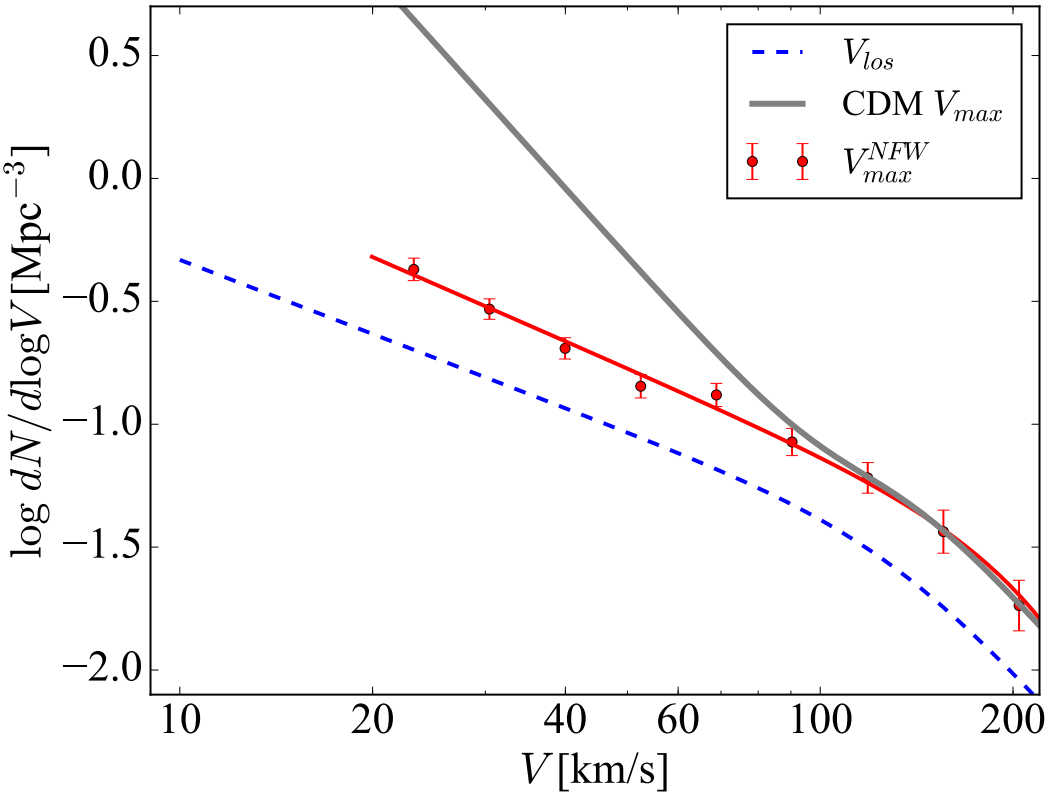

Figure 7. Galactic V_{max} function of the Local Volume. Points with error bars denote the distribution obtained by using Eq. 17 to calculate the V_{max} of each galaxy in the LV sample. The solid curve is a Schechter fit to the distribution (see Eq. 19). The dashed curve is the observed V_{los} function. The grey curve is the parametrisation of the theoretical CDM VF from K15.

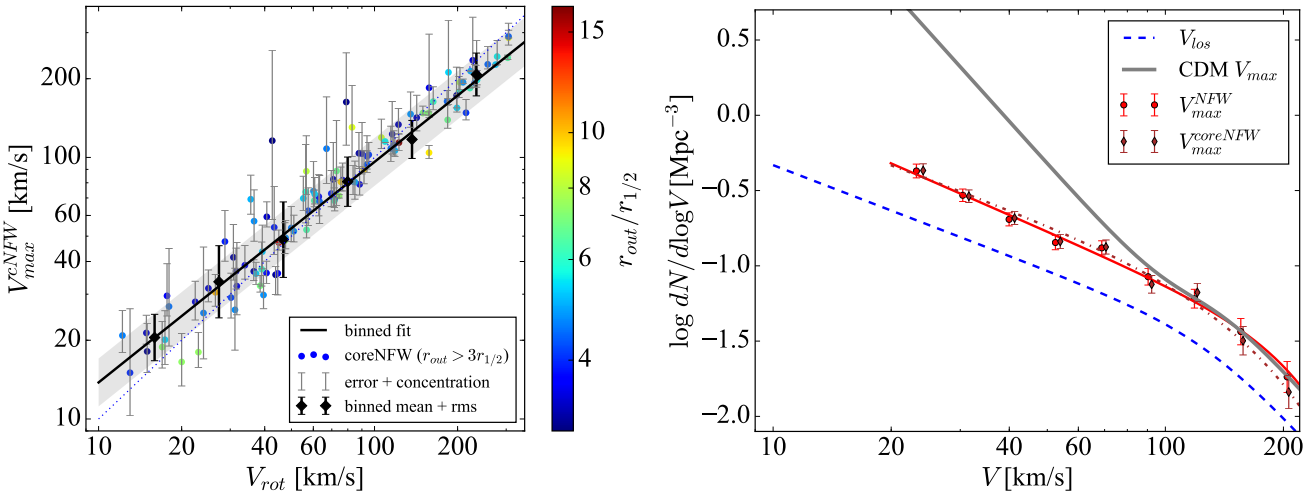

Figure 9. Left: Same as Fig. 6 assuming all haloes have flat inner cores resulting from stellar feedback. The selection of galaxies with $r_{out} > 3r_{1/2}$ ensures that the core has little effect on the resulting V_{max} compared to NFW profiles (see Fig. 5). Right: Galactic V_{max} function of the Local Volume including the effects of feedback-induced cores on density profiles. Diamonds show the result of assuming maximum cores in the coreNFW parameterisation from Read et al. (2016). Squares reproduce the result in Figure 7 which assumes NFW profiles. The dot-dashed and solid curves are Schechter fits to the NFW and coreNFW points respectively. The grey curve is the parameterisation of the CDM halo VF from K15.

fects of baryon depletion due to stellar feedback and an external UV background after reionisation.

4.2 The impact of stellar feedback and reionisation on the observed galaxy abundance

It is expected that once the universe becomes reionised at redshift $z \sim 6$, the background ultraviolet radiation field from galaxies and quasars will have a strong effect of the formation of the faintest dwarf galaxies. In DM haloes with shallow potential wells cold neutral hydrogen will be ionised and heated. The ionised gas could then escape the halo and leave a "dark galaxy" behind. These dark galaxies may contain few to no stars depending on the timescales of accretion, photo-evaporation and star formation.

Although a complete modelling of the process is extremely difficult, simplified simulations have shown that the total baryonic mass of the halo at $z = 0$ is sharply suppressed for masses below a characteristic scale $M_{\rm vir} \sim 10^{9.5}$ M$_\odot$ (Okamoto et al. 2008). The imprint of the transition should be detectable in galaxy samples of the smallest field dwarfs known to date. Therefore, the P16 sample is ideal to search for the signature of this process.

Since photo-evaporation might also affect other galaxy properties such as the extent of the HI disc, it is important to relate the baryonic mass to the depth of the potential well, using V_{max}. Figure 10 shows $M_{\rm bar}$ versus V_{max} obtained using NFW profile fitting (see Section 3.3). Two processes should be dominant in setting this relation: loss of gas due to feedback-produced outflows, and photo-evaporation due to an external UV field. The physics of these processes is quite different and there is no reason to expect a simple linear scaling of the baryon mass with halo circular velocity (in logarithmic units). A second-order polynomial least squares fit of the form $\log V_{max} = a_1 \log M_{\rm bar}^2 + a_2 \log M_{\rm bar} + a_3$ yields a negligible quadratic term, indicating that the data favour a nearly perfect linear relation between maximum circular velocity and baryonic mass.

To obtain a limit on the maximum amount of baryonic loss supported by the data, we fit a no-suppression linear model of the form

$$\log M_{\rm bar}^{nosup}(V_{max}) = a \log V_{max} + b, \quad (24)$$

as well as model with a baryonic mass suppression term,

$$M_{\rm bar}^{sup}(V_{max}) = f_{sup}(V_{max}) \times M_{\rm bar}(V_{max}), \quad (25)$$

where

$$f_{sup}(V_{max}) = 0.5 \left[1 + {\rm erf}\left(\frac{\log V_{max} - \log V_0}{\log \sigma_0}\right)\right]. \quad (26)$$

Here, V_0 is the V_{max} value where the baryonic mass is reduced by 50 per cent relative to the no-suppression model, and σ_0 is the width of the transition. We assume that a very sharp transition is unphysical and limit the width to $\log(\sigma_0/\ {\rm km\ s^{-1}}) > 1.2$, similar to the value found by Okamoto et al. (2008). Figure 10 shows the results for both models. Since the model with suppression has two free parameters, we show a family of fits which are 3-σ away from the no-suppression model using a likelihood ratio analysis.

The next step is to obtain the modified VF is to calculate the number of galaxies that are detected in surveys as a function of V_{max} and their maximum suppressed baryonic content. Assuming that the scatter in the $M_{\rm bar} - V_{max}$ relation is gaussian, the detected abundance will be reduced by half at $V_{max} = V_{crit}$, and the functional shape of the transition will be described by an error function of the form

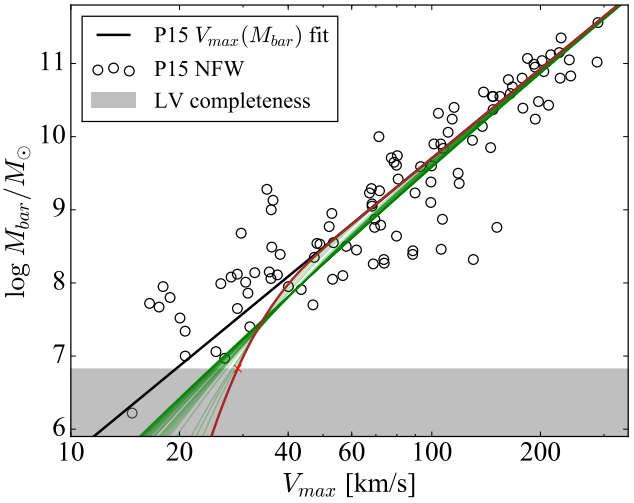

Figure 10. Relation between cold baryonic mass and V_{max} for the selected P16 galaxies. The straight line shows the no-suppression model in the form of a linear relation. The thin curves show the most extreme fits to the suppression model (Eq. 25) that are within the 3-σ allowed region when V_{crit} and σ_{crit} are allowed to vary freely. The shaded area shows the completeness limit of the Local Volume sample. The thick curve corresponds to the suppression model with the strongest effect on the observable galaxy VF. The "x" marks the value V_{crit} at which half of the galaxies in the LV are undetected assuming maximum suppression.

$$\mathcal{F}_{ext}(V_{max}) = 0.5 \left[1 + {\rm erf}\left(\frac{\log V_{max}^{sup} - \log V_{crit}}{\sqrt{2}\sigma_{\log V_{max}}}\right)\right], \quad (27)$$

where $M_{\rm bar}^{sup}$ is given by Eq. 25, $\sigma_{\log V_{max}} = 0.12$ is the logarithmic scatter in V_{max} around the linear fit, and V_{crit} is the value of V_{max} when the baryonic mass is equal to the completeness limit of the Local Volume catalog. Using the B-band limiting magnitude from Klypin et al. (2015), $\langle B - K \rangle = 2.35$ for dwarf irregulars (Jarrett et al. 2003), and $M_*/L_K = 0.6$ gives the stellar mass completeness limit, $M_{lim} = 10^{6.8}$ M$_\odot$.

In addition to photo-evaporation, DM haloes hosting star formation and energetic feedback from supernovae and stellar radiation may lose a significant fraction of their baryons through massive gas outflows (e.g., Governato et al. 2010; Brook et al. 2011; Munshi et al. 2013; Shen et al. 2014; Oñorbe et al. 2015; Trujillo-Gomez et al. 2015; Wang et al. 2015; Wheeler et al. 2015). This effect has been observed in simulations where feedback is tuned to reproduce the observed stellar mass function (Sawala et al. 2015). The loss of baryons at early times reduces the accretion rate of dark matter and hence and total mass of the halo at $z = 0$. This effect lowers the V_{max} of all dwarf haloes and produces a net shift in the velocity function.

The *maximum* possible reduction in the mass of a halo due to internal (feedback) processes can be modelled as a reduction at high redshift in the total matter abundance by a factor equal to the baryon fraction, $\Omega_{\rm bar} \to 0$. The total matter density then becomes

$$\Omega_{\rm m}^{int} = \Omega_{\rm m} - \Omega_{\rm bar}, \quad (28)$$

where $\Omega_{\rm m}$ and $\Omega_{\rm m}$ are the *Planck* total matter and baryon densities. Since the power spectrum includes a contribution from baryons, the reduction in the baryon density causes a reduction of the power given by

$$P^{int}(k) = (\Omega_{\rm DM}/\Omega_{\rm m})^2 P_{\rm DM}(k) = (\Omega_{\rm DM}/\Omega_{\rm m})^2 P(k). \quad (29)$$

Using $\Omega_{\rm m}^{int}$ and $P^{int}(k)$ in the Extended Press-Schechter formalism (Schneider et al. 2013, 2014; Schneider 2015) allows us to obtain the new feedback-modified velocity function. The result can be fit with a simple reduction of the velocities,

$$V_{max}^{int} = f_{int} V_{max}, \quad (30)$$

with $f_{int} = 0.86$. This is equivalent to a ~ 40 per cent reduction in the normalisation of the VF. The total effect from external UV photo-evaporation plus internal feedback baryon depletion on the velocity function of DM haloes is then

$$\Phi_{\rm gal}(V_{max}) = \mathcal{F}_{ext}(V_{max}^{int}/f_{int}) \times \Phi_{\rm CDM}(V_{max}^{int}/f_{int}). \quad (31)$$

Figure 11 shows the new CDM VF corrected for baryonic effects. The abundance of detected DM haloes at the lowest observed V_{max} is about five times lower than the original collisionless CDM estimate. This is, however, not enough to bring it into agreement with the observed galaxy V_{max} function in the Local Volume obtained in Section 4.1. Allowing for the maximum feedback and photoevaporation supression, the CDM velocity function is still a factor of ~ 3 above the observed V_{max} VF regardless of the assumed core/cusp nature of the density profiles.

5 COMPARISON TO PREVIOUS WORK

Brook & Shankar (2016) performed an analysis of the rotation measurement biases in the local VF using data from the ALFALFA survey (Papastergis et al. 2011). They modified the theoretical CDM velocity function using abundance matching and then applied various observational BTF relations to obtain the "observed" ALFALFA VF. They find that the definition of rotation velocity fully accounts for the large disagreement between CDM and the observed galaxy VF.

Our conclusions are strikingly different mainly due to two assumptions. First, the ALFALFA BTF relation assumed by Brook & Shankar (2016) is much shallower than what is obtained from the Local Volume. Second, abundance matching tends to place dwarf galaxies within more massive halos than what the P16 rotation curves would suggest. In this work we chose to use mass modelling as a more accurate probe of halo circular velocity than halo abundance matching.

To understand why the ALFALFA relation is shallower, we performed our analysis with the ALFALFA catalog. Using this data is more challenging because the survey is magnitude instead of volume-limited. This, combined with systematics in the faintest objects, yields a BTF relation that is poorly defined at the low-mass end. Figure 12 shows the result of fitting a linear model of the form $\log W50/2 = \alpha \log M_{\rm bar} + \beta$. To account for deviations from a power-law, we also show the binned statistics for ten equally-spaced logarithmic bins in baryon mass. The binned fit to the ALFALFA line-of-sight velocities as a function of $M_{\rm bar}$ is comparable to the fit for the Local Volume BTF relation (Eq. 2). Therefore, using the ALFALFA dataset to construct a V_{max} velocity function of the local universe using Eq. 17 would yield the same result shown in Figure 7.

Papastergis & Ponomareva (2016) compared the rotation curves of the lowest mass NIHAO hydrodynamic runs to the P16 dwarfs by matching them using H I 50 percent profile widths. They find that dwarf galaxies with large kinematic radii ($r_{out} > 1.5$ kpc) have lower V_{rot} than the NIHAO objects, and conclude that these objects cannot be explained by the simulations.

Instead, Macciò et al. (2016) argue that compared to massive galaxies, the thicker and turbulent H I discs of dwarfs lead to observed H I profile widths that fail to trace the gravitational potential of the halo. Our method relies on high-quality rotation curves for which turbulent support is included in estimating V_{out}. This should make V_{out} a better tracer of the potential. Nonetheless, the results of our analysis would not hold if it is demonstrated that rotation curves are poor tracers of the mass distribution in dwarf galaxies.

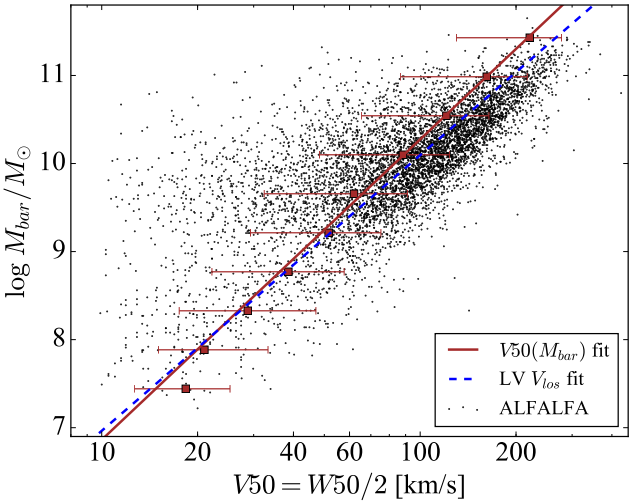

Figure 12. ALFALFA data compared to the Local Volume sample. Points represent the ALFALFA galaxies. The solid line is a linear fit to $\log V50(\log M_{\rm bar})$. Squares with error bars show indicate the mean and standard deviation of the data in uniform $\log M_{\rm bar}$ bins. The dashed line reproduces the fit to the LV line-of-sight velocities from Fig. 2. The ALFALFA fit is essentially identical to the Local Volume for $V50 < 60$ km s^{-1}.

6 CONCLUSIONS

In this paper we have performed a detailed analysis of galaxies in the Local Volume to obtain the velocity function of the dark matter haloes that host the faintest known dwarfs. We have shown that the tightly correlated Baryonic Tully-Fisher relation can be used to correct the systematic biases in rotation measurements from unresolved H I observations. Using the largest sample of high quality rotation curves together with the Local Volume catalog, we derived a V_{max} velocity function of galaxies for unmodified NFW density profiles as well as for feedback-induced cores. The observed V_{max} VF of galaxies in the Local Volume was compared to theoretical and observational estimates of the effect of photo-evaporation and stellar feedback on the theoretical CDM halo VF. Our conclusions are the following:

- The observed V_{max} velocity function of galaxies is slightly steeper than the line-of-sight VF and has a higher normalisation (due mainly to inclination effects). The slightly steeper slope is a result of the $V_{max} - V_{rot}$ relation (Fig. 6). The new V_{max} VF is still well below the theoretical CDM halo VF for scales below $V_{max} \sim 80$ km s^{-1}.
- Feedback-induced dark matter cores do not significantly affect the observed V_{max} velocity function. This occurs because a large fraction of rotation curves extend well outside the region where cores are expected to form (within 2 half-light radii), producing fits

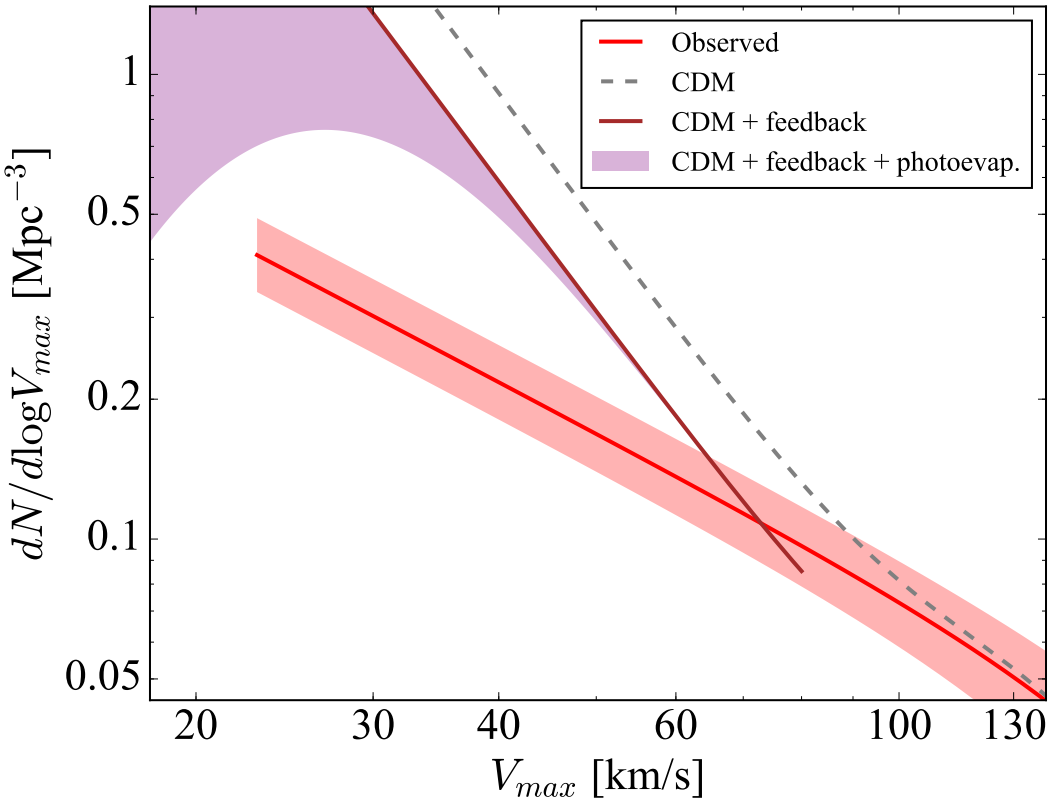

Figure 11. Theoretical CDM velocity function including the effects of stellar feedback and photoevaporation. The dashed curve is the parameterisation of the CDM halo VF from K15. The lower solid curve includes the reduction of circular velocities of haloes due feedback-powered outflows. The shaded area includes the 3-σ allowed region of suppression of halo detection due to photoevaporation from an ionising background (see Fig. 10).

with the same halo mass (and hence V_{max}) as in the case with pure NFW profiles.

- The maximum effect of stellar feedback on the CDM halo abundance can be estimated using a reduction of the cosmic baryon density and power spectrum amplitude at high redshift. The net effect is a reduction of the normalisation of the VF of ~ 40 per cent.
- Photo-evaporation of gas due to reionisation can be modelled as bend in the power-law relation between baryonic mass and halo V_{max} (Fig. 10). The break is not detected in current data but we can obtain an allowed (3-σ) limit on the reduction of halo detection due to reionisation suppression (Fig. 11).
- The combined impact of baryons through stellar feedback and photo-evaporation reduces the expected CDM halo abundance by a maximum factor of ~ 2 for halos with $V_{max} \approx 30$ km s^{-1}. This is still a factor of ~ 3 above the observed abundance of galaxies with the same circular velocity in the Local Volume. This discrepancy could point to the necessity of a modification of the cosmological predictions on small scales. Possible alternatives are provided by warm or self-interacting dark matter models.

Finally, we would like to note that our analysis rests on the customary assumption that extended HI rotation curve measurements (including turbulent corrections) are a good probe of the potential of the dark matter halo hosting the galaxy. If this assumption was shown to be invalid at dwarf galaxy scales, our conclusions would change accordingly. In a future paper we will explore this possibility using hydrodynamic simulations.

In the next paper in this series (Schneider et al., in prep) we explore the velocity functions predicted by alternative dark matter models, including baryonic effects, and compare them to the observed V_{max} VF obtained using the methods described here.

7 ACKNOWLEDGEMENTS

We would like to thank Anatoly Klypin for insightful discussions, and Andrea Macciò and Aaron Dutton for generously providing their NIHAO data. A.S. acknowledges support from the Swiss National Science Foundation (PZ00P2_161363).

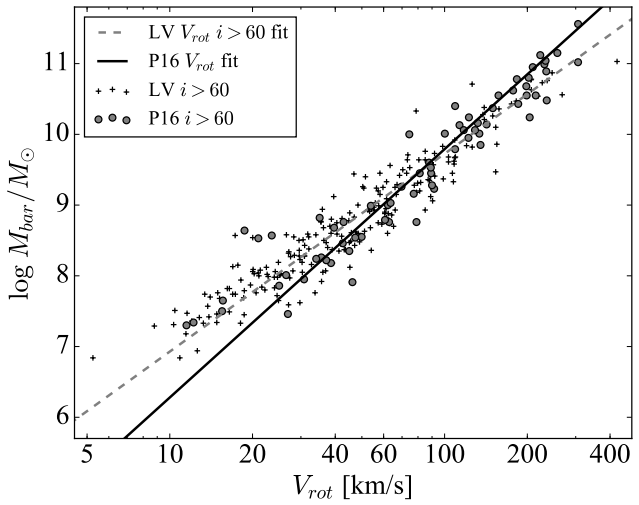

Figure A1. BTFR of the high-inclination objects from the LV and P16 samples. The solid circles show the P16 galaxies, while the crosses represent the LV galaxies. The solid line is the fit to the full P16 sample from Eq. 3, while the dashed line is a linear fit to the high-inclination LV objects.

APPENDIX A: INCLINATION UNCERTAINTIES

Figure A1 shows the BTF relations of the high-inclination ($i > 60$) LV and P16 subsamples. The inclination uncertainty in these objects is minimised compared to the full samples. Both the high-inclination LV and P16 dwarf galaxies have significantly lower rotation velocities than the full samples. As discussed by Papastergis et al. (2016), this arises because the stellar discs of dwarfs are thicker and their inclination is easily underestimated, resulting in an overestimate of the deprojected rotation velocity.

To avoid this systematic effect in our analysis we used the line-of-sight rotation velocity of the LV galaxies. In addition, removing the inclination errors in the P16 sample would reduce the average V_{out} at a fixed $M_{\rm bar}$, allowing for lower mass haloes to be fit to the same galaxies. This would have the overall effect of a systematic shift in the observed V_{max} VF towards smaller circular velocities, making the disagreement with CDM predictions even worse.

APPENDIX B: SENSITIVITY OF THE RESULTS TO SAMPLE SELECTION

Figure B1 shows the sensitivity of the linear fit from Eq. 16 to changes in the minimum value of the relative rotation curve extent, $r_{out}/r_{1/2}$, allowed in the P16 sample selection. The figure shows the slope and intercept of the fit obtained from binning the error-weighted V_{max} values as was done in Figure 6.

The observed variation in the fit parameters is relatively small and the largest deviations in the slope are compensated by changes in the intercept which result in a fit that is largely insensitive to the data selection.

To check the robustness of the second sample cut, we plot in Figure B2 the variation of the same parameters when the maximum allowed contribution from baryons to the circular velocity, $(GM_{bar}/r_{out})/V_{out}^2$, is varied.

Although the slope and intercept vary considerably for values $(GM_{bar}/r_{out})/V_{out}^2 < 0.2$, the intercept increases while the slope decreases to produce a relatively small net change in the predictions of the model.

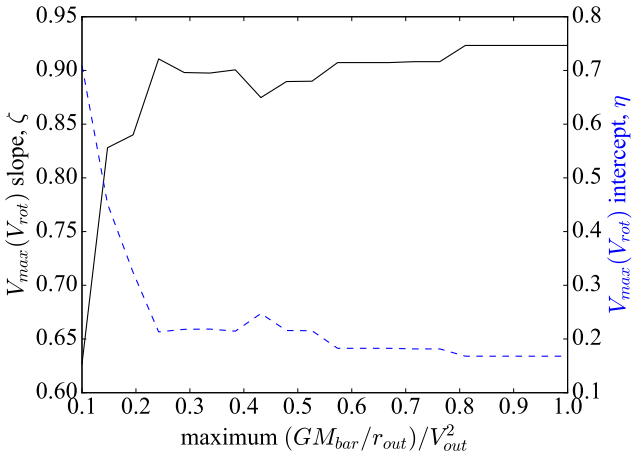

Figure B2. Effect of varying the maximum allowed contribution from the baryonic mass to the circular velocity. The left axis and solid line correspond to the slope, ζ, and the right axis and dashed line show the intercept, η. Only cuts which preserve more than 60 data points are shown.

APPENDIX C: COMPARING TO OTHER PARAMETERISATIONS OF CORED HALO PROFILES

The Di Cintio et al. (2014) (DC14) parameterisation of the DM density profile of galaxies including feedback-induced cores has been extensively used in the literature. In this work we used instead the fit by Read et al. (2016) (the "coreNFW" profile) to evaluate the effect of DM cores on the observed V_{max} velocity function. Figure C1 shows a comparison of the two fits applied to a simulation from the MAGICC suite (Di Cintio et al. 2014). Since the DC14 fit depends critically on the ratio $M_{\rm star}/M_{\rm vir}$, we used the values reported for the simulation by Di Cintio et al. (2014). For the coreNFW fit we took the half-light radius of the same simulation from Brook et al. (2012), assumed a flat core with $n = 1$, and varied the concentration to obtain a good fit. The figure shows that the coreNFW fit is also a good description of the DM core formed in the simulation.

This example further confirms the validity of the coreNFW profile for accurately capturing the extent of feedback-induced cores in hydrodynamic simulations. Our results are therefore independent of our choice of cored profile model.

REFERENCES

Arraki K. S., Klypin A., More S., Trujillo-Gomez S., 2014, MNRAS, 438, 1466
Boylan-Kolchin M., Bullock J. S., Kaplinghat M., 2011, MNRAS, 415, L40
Bradford J. D., Geha M. C., Blanton M. R., 2015, ApJ, 809, 146
Brook C. B. et al., 2011, MNRAS, 415, 1051
Brook C. B., Shankar F., 2016, MNRAS, 455, 3841
Brook C. B., Stinson G., Gibson B. K., Wadsley J., Quinn T., 2012, MNRAS, 424, 1275
Brooks A. M., Kuhlen M., Zolotov A., Hooper D., 2013, ApJ, 765, 22
Brooks A. M., Zolotov A., 2014, ApJ, 786, 87
Di Cintio A., Brook C. B., Dutton A. A., Macciò A. V., Stinson G. S., Knebe A., 2014, MNRAS, 441, 2986
Diemand J., Kuhlen M., Madau P., 2007, ApJ, 667, 859
Dutton A. A., Macciò A. V., 2014, MNRAS, 441, 3359

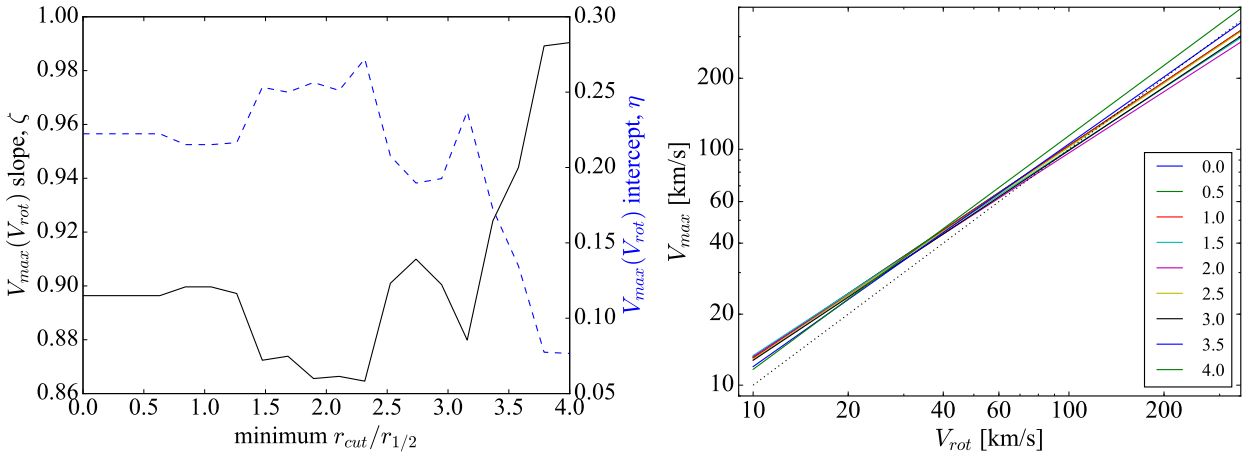

Figure B1. Effect of varying the minimum $r_{out}/r_{1/2}$ of the P16 sample on the linear fit to Eq. 16. Left: the left axis and solid line correspond to the slope, ζ, and the right axis and dashed line show the intercept, η. Right: comparison of the models. The value of $r_{out}/r_{1/2}$ for each model is indicated in the legend. The dotted line shows $V_{max} = V_{rot}$. Only cuts which preserve more than 60 data points are shown. The variation in the fit parameters is relatively small, with the slope changes usually compensated by changes in the intercept to produce a robust fit at low velocities.

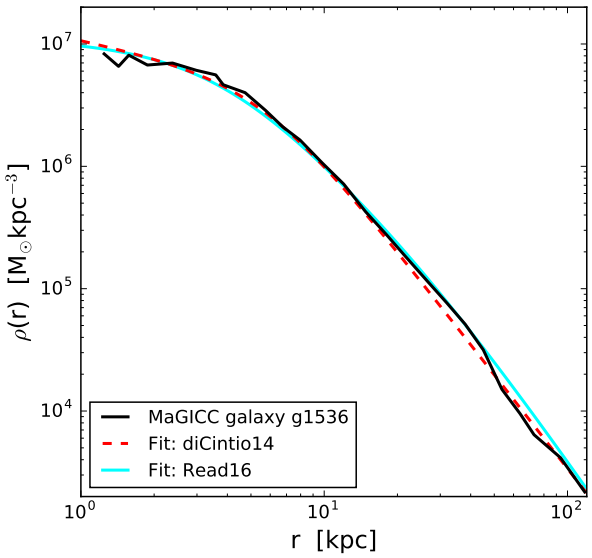

Figure C1. Comparison of the Di Cintio et al. (2014) and Read et al. (2016) cored DM halo profile parameterisations. The solid black line is the density profile of the hydrodynamical galaxy simulation g1536 from Di Cintio et al. (2014). The dashed and solid curves are the DC14 and coreNFW fits respectively.

Gnedin N. Y., 2000, ApJ, 542, 535
Governato F. et al., 2010, Nature, 463, 203
Governato F. et al., 2012, MNRAS, 422, 1231
Heitmann K. et al., 2016, ApJ, 820, 108
Hellwing W. A., Frenk C. S., Cautun M., Bose S., Helly J., Jenkins A., Sawala T., Cytowski M., 2016, MNRAS, 457, 3492
Hoeft M., Yepes G., Gottlöber S., Springel V., 2006, MNRAS, 371, 401
Jarrett T. H., Chester T., Cutri R., Schneider S. E., Huchra J. P., 2003, AJ, 125, 525
Karachentsev I. D., Makarov D. I., Kaisina E. I., 2013, AJ, 145, 101
Klypin A., Karachentsev I., Makarov D., Nasonova O., 2015, MNRAS, 454, 1798
Klypin A., Kravtsov A. V., Valenzuela O., Prada F., 1999, ApJ, 522, 82
Klypin A. A., Trujillo-Gomez S., Primack J., 2011, ApJ, 740, 102
Macciò A. V., Udrescu S. M., Dutton A. A., Obreja A., Wang L., Stinson G. R., Kang X., 2016, MNRAS, 463, L69
Mashchenko S., Wadsley J., Couchman H. M. P., 2008, Science, 319, 174
McGaugh S. S., 2012, AJ, 143, 40
Moore B., Ghigna S., Governato F., Lake G., Quinn T., Stadel J., Tozzi P., 1999, ApJL, 524, L19
Munshi F. et al., 2013, ApJ, 766, 56
Nagashima M., Okamoto T., 2006, ApJ, 643, 863
Navarro J. F., Frenk C. S., White S. D. M., 1997, ApJ, 490, 493
Oñorbe J., Boylan-Kolchin M., Bullock J. S., Hopkins P. F., Kereš D., Faucher-Giguère C.-A., Quataert E., Murray N., 2015, MNRAS, 454, 2092
Okamoto T., Gao L., Theuns T., 2008, MNRAS, 390, 920
Papastergis E., Adams E. A. K., van der Hulst J. M., 2016, ArXiv e-prints
Papastergis E., Giovanelli R., Haynes M. P., Shankar F., 2015, A&A, 574, A113
Papastergis E., Martin A. M., Giovanelli R., Haynes M. P., 2011, ApJ, 739, 38
Papastergis E., Ponomareva A. A., 2016, ArXiv e-prints
Read J. I., Agertz O., Collins M. L. M., 2016, MNRAS, 459, 2573
Read J. I., Iorio G., Agertz O., Fraternali F., 2016, MNRAS, 462, 3628
Reed D. S., Smith R. E., Potter D., Schneider A., Stadel J., Moore B., 2013, MNRAS, 431, 1866
Sawala T. et al., 2016, MNRAS, 457, 1931
Sawala T. et al., 2015, MNRAS, 448, 2941
Schneider A., 2015, MNRAS, 451, 3117
Schneider A., Anderhalden D., Macciò A. V., Diemand J., 2014, MNRAS, 441, L6
Schneider A., Smith R. E., Reed D., 2013, MNRAS, 433, 1573
Shen S., Madau P., Conroy C., Governato F., Mayer L., 2014, ApJ,

792, 99
Somerville R. S., 2002, ApJL, 572, L23
Springel V. et al., 2005, Nature, 435, 629
Teyssier R., Pontzen A., Dubois Y., Read J. I., 2013, MNRAS, 429, 3068
Tikhonov A. V., Klypin A., 2009, MNRAS, 395, 1915
Tollet E. et al., 2016, MNRAS, 456, 3542
Trujillo-Gomez S., Klypin A., Colín P., Ceverino D., Arraki K. S., Primack J., 2015, MNRAS, 446, 1140
Trujillo-Gomez S., Klypin A., Primack J., Romanowsky A. J., 2011, ApJ, 742, 16
Wang L., Dutton A. A., Stinson G. S., Macciò A. V., Penzo C., Kang X., Keller B. W., Wadsley J., 2015, MNRAS, 454, 83
Wheeler C., Oñorbe J., Bullock J. S., Boylan-Kolchin M., Elbert O. D., Garrison-Kimmel S., Hopkins P. F., Kereš D., 2015, MNRAS, 453, 1305
Zavala J., Jing Y. P., Faltenbacher A., Yepes G., Hoffman Y., Gottlöber S., Catinella B., 2009, ApJ, 700, 1779
Zolotov A. et al., 2012, ApJ, 761, 71

This paper has been typeset from a TEX/ LATEX file prepared by the author.